



ELSEVIER

Contents lists available at ScienceDirect

## Journal of Sound and Vibration

journal homepage: [www.elsevier.com/locate/jsv](http://www.elsevier.com/locate/jsv)

# Damping of structural vibrations in beams and elliptical plates using the acoustic black hole effect

V.B. Georgiev<sup>a,\*</sup>, J. Cuenca<sup>a</sup>, F. Gautier<sup>a</sup>, L. Simon<sup>a</sup>, V.V. Krylov<sup>b</sup>

<sup>a</sup> Laboratoire d'Acoustique de l'Université du Maine, CNRS, Av. O. Messiaen, Le Mans 9, France

<sup>b</sup> Department of Aeronautical and Automotive Engineering, Loughborough University, Ashby Road, Loughborough, Leicestershire LE11 3TU, UK

## ARTICLE INFO

### Article history:

Received 23 March 2010

Received in revised form

30 November 2010

Accepted 1 December 2010

Handling Editor: H. Ouyang

Available online 1 February 2011

## ABSTRACT

Flexural waves in beams and plates slow down if their thickness decreases. Such property was used in the past for establishing the theory of acoustic black holes (ABH). The aim of the present paper is to establish reliable numerical and experimental approaches for designing, modelling and manufacturing an effective passive vibration damper using the ABH effect. The effectiveness of such vibration absorbers increases with frequency. Initially, the dynamic behaviour of an Euler–Bernoulli beam is expressed using the Impedance Method, which in turn leads to a Riccati equation for the beam impedance. This equation is numerically integrated using an adaptive Runge–Kutta–Fehlberg method, yielding the frequency- and spatially-dependent impedance matrix of the beam, from which the reflection matrix is obtained. Moreover, the mathematical model can be extended to incorporate an absorbing film that assists for reducing reflected waves from the truncated edge. Therefore, the influence of the geometrical and material characteristics of the absorbing film is then studied and an optimal configuration of these parameters is proposed. An experiment consisting of an elliptical plate with a pit of power-law profile placed in one of its foci is presented. The elliptical shape of the plate induces a complete focalisation of the waves towards ABH in case they are generated in the other focus. Consequently, the derived 1-D method for an Euler–Bernoulli beam can be used as a phenomenological model assisting for better understanding the complex processes in 2-D elliptical structure. Finally, both, numerical simulations and experimental measurements show significant reduction of vibration levels.

© 2010 Elsevier Ltd. All rights reserved.

## 1. Introduction

Damping of structural vibrations of beams and plates has always been a challenging aim for many researchers and engineers. One of the methods for achieving this goal is by reducing wave reflections from boundaries of structures under test by treating their ends. In this regard, the fact that flexural waves in beams and plates slow down if their thickness decreases was successfully used by Mironov for establishing the theory of **Acoustic Black Holes** (ABH) [1]. The main idea of this approach is to use a power-law relationship between local thickness  $h$  and the distance from the edge  $x$ , in the form

$$h(x) = \varepsilon x^m \quad (m \geq 2), \quad (1)$$

in order to reduce the local phase velocity. Furthermore, it can be shown that the travel time needed for a wave to reach the edge of a beam can be infinite when the truncated thickness of the profile tends to zero. Therefore, under such

\* Corresponding author.

E-mail addresses: [vb\\_georgiev@yahoo.com](mailto:vb_georgiev@yahoo.com), [Vasil.Georgiev@univ-lemans.fr](mailto:Vasil.Georgiev@univ-lemans.fr) (V.B. Georgiev).

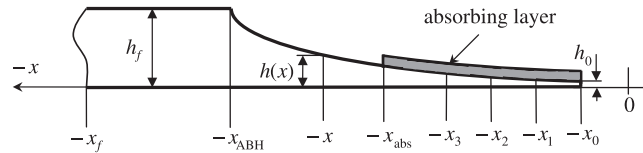


Fig. 1. One-dimensional ABH configuration, the corresponding geometrical dimensions are given in Table 1.

conditions the flexural waves stop propagating and the reflection coefficient becomes equal to zero. This is the basic principle of ABH as described by Mironov.

Nevertheless, the practical implementation of this idea is a complicated task because of manufacturing difficulties. Despite the high precision of modern cutting machines, manufactured beams and plates with power-law profiles always exhibit truncations at certain distance  $x_0$  from the coordinate origin, with a non-zero edge thickness  $h_0$  (see e.g. Fig. 1). This is why a reflected wave from a truncated edge always occurs, which partly cancels the effect of ABH and makes its practical application unattractive. However, a recently proposed approach by Krylov et al. [2–4] has combined the use of power-law profile wedge (ABH) with a thin absorbing film with length  $x_{\text{abs}} - x_0$  (see Fig. 1) covering fully or partially the treated area, leading to the so-called acoustic black hole effect. Thus, the additional use of a conventional damping technique could overcome to some extent the undesirable consequences of the truncated thickness profile.

In more details, Krylov et al. [2–4] have used a geometrical acoustic approach to describe the propagation of flexural waves towards a free edge. The effect of a thin absorbing film was taken into account using the model of Ross–Ungar–Kerwin [5] for constrained layer damping in the special case of extensional damping (no constraining layer). As a result, the reflection coefficient was analytically expressed as simplified formulae for different power-law profiles of order  $m=2, 3, 4$  and for a sinusoidal profile [2]. More detailed expression of reflection coefficient is given in Ref. [3], where the effect of thicker absorbing films was taken into consideration. Furthermore, the first experimental results regarding the use of ABH along with adhesive material as an effective vibration absorber were reported by Krylov and Winward [4]: measurements of driving-point mobility functions of a quadratic steel plate with ABH placed at the edges were of primary interest for the authors. The frequency response functions showed significant reduction of mobility in the high frequency range for the plate which power-law profile was covered by an adhesive stripe, as compared to the same plate without absorbing material. Later on, experiments on tapered rods with power-law profiles [6] demonstrated the damping of flexural vibrations in one-dimensional structures and its application for reducing impact-induced vibrations in tennis and badminton racquets [7]. Thus, the combination between ABH and additional damping material was experimentally validated as a promising measure for vibration reduction. Preliminary results to the present work were published in Ref. [8] in the case of elliptical plates where an ABH was placed in the inner domain and not at the boundary of the structure, taking advantage of a focalisation effect.

A similar method for attenuating structural wave reflections at the edges of bars and plates by using graded impedance interfaces has been reported by Vemula et al. [9]. It is known that the energy reflection in inhomogeneous elastic materials is caused by mismatch of impedance characteristics between different regions. The idea of the method is to change gradually the impedance at the edge by using a combination of different plates of the same thickness with specific impedance properties. Thus, gradually modifying the impedance properties at the end of the steel plate, part of vibration energy was successfully damped in the range from 2 to 10 kHz. The similarity between ABH and graded impedance interfaces is in modifying the impedance properties near the edge of the beam or plate. However, the latter approach requires a relatively large number of different material layers in order to design a smooth impedance curve, which makes it difficult for practical application.

In the light of above-mentioned previous research, the aim of this paper is twofold. Firstly, a reliable numerical method for modelling of ABH in 1-D beam structures, which is not limited by the hypothesis of geometrical acoustics, is to be established. This will allow optimising geometrical and material parameters of the absorbing film in order to decrease reflection coefficient from the truncated edge to its optimal values. Secondly, an experimental method for damping flexural vibrations in 2-D structures using ABH and wave focusing effects is to be developed. It is achieved by using an axisymmetric pit of power-law profile centred on one of the focal points of an elliptical plate. The efficiency of this approach is evaluated experimentally comparing driving-point mobilities of elliptical plates with and without ABH. To the best of authors' knowledge all above-mentioned aims represent new findings in the area of ABH theory.

Note that the manufacturing process of producing an ABH is very complex because of the very small truncation thickness that must be achieved, in the order of 1–10  $\mu\text{m}$  even less, and at the same time following the power-law profile. This process has been implemented successfully for an elliptical plate but not so effectively for a beam structure. On the other hand, building 2-D theoretical model of an ABH is related with substantial analytical difficulties, therefore at this stage the 1-D theoretical model is used for better understanding the physics of ABH in the considered 2-D system.

What follows, in Section 2 the basic principles of the numerical model of a 1-D ABH are presented. In Section 3, the results of numerical simulations are shown. In more details, Section 3.1 illustrates ABH effect, whereas Section 3.2 deals with a parametric study that allows an optimisation of the geometrical and material parameters of the absorbing film. Section 4 encompasses the experimental investigation of elliptical plates with and without ABH, showing the applicability of the concept. Comparisons with numerical results are included as well.

## 2. Modelling of one-dimensional ABH

As was mentioned above, a 1-D ABH is a non-uniform beam having a power-law profile. This 1-D ABH can be extended to a 2-D configuration consisting of an axisymmetric pit which thickness gradually decreases to (theoretically) zero towards its centre according to the 1-D thickness profile. Furthermore, the shape of an elliptical plate induces a focalisation of the waves towards one of its foci if the excitation is applied in the other focus. Thus, considering an inner ABH placed in one of the foci, all the generated waves in the other focus will reach it either directly or after reflections from the free edges. The waves excited in this way could be considered as vibrational rays starting from the driving focus and ending to the damped focus, see Fig. 2. Note that placing the ABH in the inner part of a plate instead of an edge has not been investigated in the previous ABH studies and is one of the originality of the present approach. In this regard, the 1-D ABH model can be considered as a phenomenological model for the complex 2-D elliptical configuration.

The non-uniform beam, shown in Fig. 1 and having an axis  $x$ , represents the 1-D ABH under consideration. The non-uniform region is between  $x_{ABH}$  and  $x_0$  whereas the absorbing film is between  $x_{abs}$  and  $x_0$ . The coordinate  $x_f$  denotes an arbitrary point in the uniform region. The varying thickness is given by Eq. (1) and the thickness at the end (at  $x_0$ ) is given by  $h_0 = \epsilon x_0^m$ .

The 1-D ABH model is based on classical beam theory: Euler–Bernoulli hypotheses are assumed [10]. The vibrational state of the beam can be described by four variables: the displacement  $w$ , the local slope  $\theta$ , the shear force  $F$  and the bending moment  $M$ . Harmonic motion is assumed (time factor  $e^{i\omega t}$  is supposed) and all variables depend only on the spatial coordinate  $x$ . In this context, a state vector  $\mathbf{X}$  consisting of the four variables can be written as follows:

$$\mathbf{X} = [w \ \theta \ F \ M]^T \tag{2}$$

and

$$\frac{\partial \mathbf{X}}{\partial x} = \mathbf{H}\mathbf{X}, \tag{3}$$

where

$$\mathbf{H} = \begin{bmatrix} \mathbf{H}_1 & \mathbf{H}_2 \\ \mathbf{H}_3 & \mathbf{H}_4 \end{bmatrix}, \quad \mathbf{H}_1 = \begin{bmatrix} 0 & 1 \\ 0 & 0 \end{bmatrix}, \quad \mathbf{H}_2 = \begin{bmatrix} 0 & 0 \\ 0 & 1/E_1 I_1 \end{bmatrix}, \quad \mathbf{H}_3 = \begin{bmatrix} -\rho_1 A_1 \omega^2 & 0 \\ 0 & 0 \end{bmatrix}, \quad \mathbf{H}_4 = \begin{bmatrix} 0 & 0 \\ -1 & 0 \end{bmatrix},$$

$\rho_1$  is the material density of the beam,  $A_1 = bh$  is the area of the beam’s cross-section,  $E_1$  is Young’s modulus of the beam, and  $I_1 = bh^3/12$  is the moment of inertia of the beam’s cross-section.

Thus, Eq. (3) is a compact formulation of the Euler–Bernoulli model [11,12]. Notes and relationships useful for the present study are given in Appendix A. The state vector is composed of two kinematic and two force variables, which allows defining the local impedance matrix  $\mathbf{Z}$

$$[F \ M]^T = j\omega \mathbf{Z} [w \ \theta]^T, \quad \text{with } \mathbf{Z} = \begin{bmatrix} Z_1 & Z_2 \\ Z_3 & Z_4 \end{bmatrix}. \tag{4}$$

It can be shown that the impedance matrix  $\mathbf{Z}$  is the solution of the Riccati equation (see Appendix A)

$$\frac{\partial \mathbf{Z}}{\partial x} = -\mathbf{Z}\mathbf{H}_1 - j\omega \mathbf{Z}\mathbf{H}_2 \mathbf{Z} + \frac{\mathbf{H}_3}{j\omega} + \mathbf{H}_4 \mathbf{Z}. \tag{5}$$

Note: Matrices  $\mathbf{H}_1$ ,  $\mathbf{H}_2$ ,  $\mathbf{H}_3$ , and  $\mathbf{H}_4$  are characteristic matrices of the propagating medium given in Appendix A. If impedance  $\mathbf{Z}$  can be specified at one point of the medium, then solving Eq. (4) gives the way to compute  $\mathbf{Z}$  at any coordinate and to

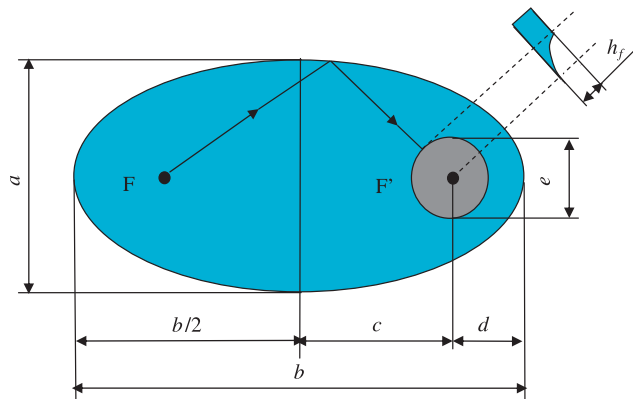


Fig. 2. Model of elliptical plate flexural vibrations approximated by 1-D vibration rays.

derive the response of the medium to any excitation force. This is the basic principle of the Impedance Matrix Method, as it is used for solving multimodal propagation in acoustic waveguides [13].

Once the structural impedance  $\mathbf{Z}$  is obtained, the reflection matrix  $\mathbf{R}$  ( $2 \times 2$ ) can be easily defined using a standard wave approach (see Appendix A)

$$\mathbf{R} = [j\omega\mathbf{Z}\mathbf{E}_2 - \mathbf{E}_4]^{-1}[\mathbf{E}_3 - j\omega\mathbf{Z}\mathbf{E}_1], \quad (6)$$

the matrices  $\mathbf{E}_1$ ,  $\mathbf{E}_2$ ,  $\mathbf{E}_3$ , and  $\mathbf{E}_4$  being given in Appendix A. The scalar components,  $R_1$ ,  $R_2$ ,  $R_3$ , and  $R_4$  of the reflection matrix represent the reflection and coupling between evanescent and propagating flexural waves in the beam.  $R_1$  corresponds to propagating waves whereas  $R_4$  corresponds to evanescent waves. The coupling between these two types of waves is characterised by  $R_2$  and  $R_3$ .

In 1-D ABH model the damping has two origins. (i) The visco-elastic and thermo-elastic damping inside the beam material. This kind of damping can be modelled by a complex Young's modulus  $E_1$ , which can be introduced in Eq. (A.2) using the loss factor  $\eta_1$  of beam material. (ii) Damping which can be added by a thin absorbing layer having Young's modulus  $E_2$  and loss factor  $\eta_2$ . The model developed in this study can be extended in order to include this additional damping effect due to the absorbing film.

The Ross–Ungar–Kerwin model [5] for constrained layer damping in the special case of extensional damping (no constraining layer) is employed here, as is done by Krylov [3]. The complex bending stiffness of the composite beam (beam covered by an absorbing film) can be expressed using the bending stiffness of the beam only, the phase velocity of flexural waves of the composite beam is to be computed (see Appendix B).

### 3. Numerical simulations

#### 3.1. Numerical method

The efficiency of ABH is estimated by the reflection matrix  $\mathbf{R}$ , which can be computed from the impedance matrix  $\mathbf{Z}$ , as shown in Eq. (5). The latter is the solution of Eq. (4), computed with the boundary conditions  $\mathbf{Z}(x_0)=0$ , describing the fact that the end of the beam at  $x=x_0$  is free. The numerical integration procedure of Eq. (4) employs an adaptive Runge–Kutta–Fehlberg (RKF) method [14]. Because of the widely varying scale of the problem (the thickness of the beam is supposed to vary between  $h_f=1.5$  mm and  $h_0(-0.01) \approx 1.16$   $\mu\text{m}$ , for the characteristics given in Table 1) such an adaptive approach is much more convenient than the classical method using a constant integration step. The adaptive RKF method is a numerical scheme of order 5, which uses two estimates of the solutions obtained with schemes of orders 4 and 5 [15]. The approximate values of the solution,  $y_{n+1}$  of order 4 and  $y_{n+1}^*$  of order 5, and their difference

$$e_{n+1} = y_{n+1} - y_{n+1}^*, \quad (7)$$

can be interpreted as an estimate of the local error associated with the less accurate solution  $y_{n+1}^*$  [15]. Thus,  $e_{n+1}$  is used to adjust the integration step and to keep the magnitude of the local error below the prescribed tolerance.

#### 3.2. Illustration of the ABH effect

Numerical simulations are presented for the beam defined by Fig. 1 and Table 1.

Fig. 3 shows the ABH effect by means of the scalar impedance  $Z_1$  (solid curve). For example, reducing the thickness of the beam makes the impedance curve decrease and the distance between impedance peaks become shorter towards the sharp end. Moreover, the impedance  $Z_1$  oscillates around the impedance  $Z_1^{\text{ref}}$  of a reference beam whose reflection matrix is set up to zero. The impedance matrix of the reference non-uniform beam can be calculated from the following expression:

$$\mathbf{Z}^{\text{ref}} = \frac{1}{j\omega} \mathbf{E}_3 \mathbf{E}_1^{-1}, \quad (8)$$

**Table 1**

Geometrical and material characteristics of the beam under consideration.

Geometrical characteristics	Characteristics of material
$x_0 = -0.01$ m	<i>Beam</i>
$x_{\text{ABH}} = -0.06$ m	$E_1 = 210$ GPa
$x_f = -0.08$ m	$\rho_1 = 7800$ kg/m <sup>3</sup>
	$\eta_1 = 0.001$
	<i>Abs. film</i>
$h_f = 0.0015$ m	$E_2 = 0.5$ GPa
$b = 0.0015$ m	$\rho_2 \approx 950$ kg/m <sup>3</sup>
$m = 4$	$\eta_2 = 0.05$

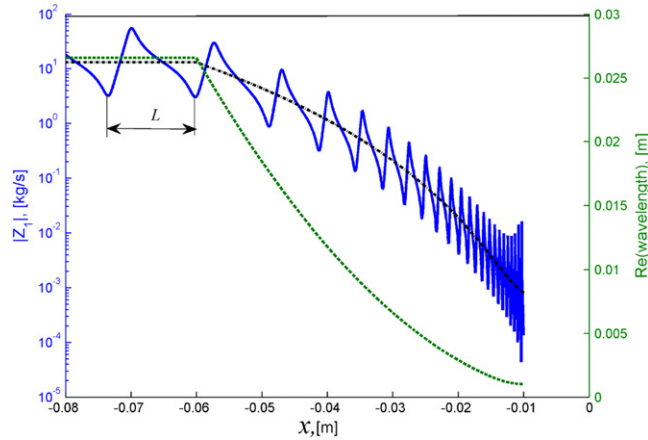


**Fig. 3.** Impedance  $Z_1$  (solid curve), wavelength (dashed curve) of a beam with ABH covered by a 10  $\mu\text{m}$  thick absorbing film; and impedance  $Z_1^{\text{ref}}$  (dash-dotted curve) of a reference beam having a reflection matrix equal to zero, calculated at 20 kHz.

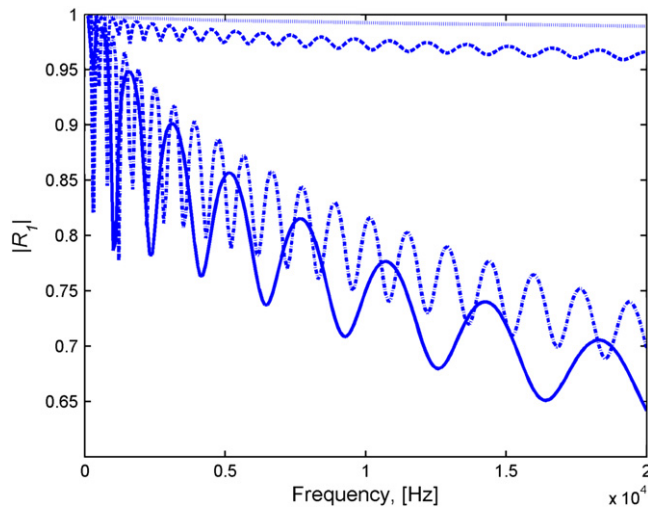


**Fig. 4.** Reflection coefficient  $R_1$  as a function of frequency for a beam with ABH and 700  $\mu\text{m}$  absorbing film (solid curve) and 10  $\mu\text{m}$  absorbing film (dash-dotted curve); ABH only (dashed curve) without absorbing film; and for a uniform beam with 700  $\mu\text{m}$  absorbing film (dotted curve).

where the matrices  $\mathbf{E}_1$  and  $\mathbf{E}_3$  are given in Appendix A. These oscillations depend on the profile's sharpness defined by the parameter  $\varepsilon$ , and the truncation distance  $x_0$ . It can be shown that at smaller values for  $\varepsilon$  and  $x_0$  the impedance  $Z_1$  tends to the impedance of the reference beam  $Z_1^{\text{ref}}$ .

In the uniform part of the beam the distance between two resonant peaks  $L$  is equal to one half of the wavelength,  $L = \lambda(x)/2$ . In the area of ABH the wavelength (dashed curve) continuously changes proportionally to the phase velocity of flexural waves. In this region the distance between two impedance peaks is roughly one half of the local wavelength,  $L \approx \lambda(x)/2$ , measured in the centre of this spatial area. In case of an ABH whose profile is without truncation, the wavelength tends to zero. Therefore, ABH could be likened to an accumulation point (all values of the wavelength form a set of an infinite amount of numbers whose limit point is zero). In practical cases, the truncation and the thickness of absorbing film define a minimal value of the wavelength.

In Fig. 4 the reflection coefficient  $R_1$  is presented as a function of frequency in order to illustrate ABH effect. It is shown that reflection coefficient  $R_1$  for a beam with ABH covered by 700  $\mu\text{m}$  (solid curve) and 10  $\mu\text{m}$  (dash-dotted curve) are, respectively, 35% and 30% reduced at 20 kHz, whereas for a beam with ABH only, without any absorbing film (dashed curve), this reduction is 3% only, and for a uniform beam covered by 700  $\mu\text{m}$  absorbing film it is even smaller—around 1.5%. Therefore, the ABH effect leads to a much more noticeable decrease of reflected waves compared to any individual treatment of the beam—ABH only or damping treatment only. It has been shown that the wavelength in the area of ABH decreases (see Fig. 3) due to the power-law profile. Besides, the wavelength is inversely proportional to the square root of

frequency, thus, at high frequencies the wavelength is further reduced, which leads to reduction of reflected waves as well. Note that the oscillations of the reflection coefficient decrease and their periodicity becomes larger when the frequency is increased. Therefore, at frequencies tending to infinity the reflection coefficient should not exhibit any oscillations. The origin of these oscillations might be due to the sharpness and length of the profile.

### 3.3. Parametric study

Using the data mentioned in Table 1, a parametric study is proposed in order to define the optimal parameters of the absorbing film at which the reflection coefficient  $R_1$  becomes minimal. ABH and absorbing film dissipate vibration energy together but using different mechanisms. The absorbing film assists for overcoming disadvantages due to the truncation, thus, the most important area is near the truncation. The effect of absorbing film is introduced by modifying the loss factor of composite beam (beam+abs. layer), which means that its main mechanism for further reducing the reflection coefficients is simply damping of propagating waves before they can reach the truncated edge. However, the absorbing film increases the thickness of power-law profile and reduces the effect of ABH. For example, adding absorbing film leads to an increase in phase velocity and wavelength in the areas where its thickness is comparable or larger to that of the beam, see Fig. 5(a). Therefore, the use of absorbing film in the area of ABH is not straightforward. This is why it is important to establish some efficient rules to optimise thickness and length of the absorbing film. In the following analysis, by varying the geometrical and material characteristics of the absorbing film, the rules are established for specifying thickness, length and loss factor of the absorbing film, which provides a minimum value of the reflection coefficient  $R_1$  and, consequently, of the reflected waves.

#### 3.3.1. Thickness of absorbing film

When dissipation characteristics are under consideration, the most relevant parameter is the loss factor of the compound beam (beam with ABH+absorbing film). In this regard, the ratio between imaginary and real parts of the wavelength gives an estimation of the loss factor of the compound beam. Fig. 5(b) shows that adding absorbing film results in an extremum in the loss factor compared to the constant one for the beam without absorbing film. The position of this maximum can be controlled by the thickness of the absorbing film. For example, at thickness of  $700 \mu\text{m}$  the maximum of the loss factor is located at around  $x = -0.023 \text{ m}$ , at thickness of  $100 \mu\text{m}$ , respectively, at  $x = -0.013 \text{ m}$ . Therefore, increasing the thickness of the absorbing film makes the maximum shift towards thicker part of the beam and vice versa. Note that the maximal value of the loss factor does not change when the thickness of the absorbing film varies. Thus, the position of the extremum is governed by the ratio between the thickness of the absorbing film and the thickness of the power-law profile. The minimal reflection coefficient corresponds to a thickness of  $40 \mu\text{m}$ . In other words, when the extremum of the loss factor is positioned at the truncation distance by choosing a proper value of the thickness of the absorbing film, the reflection of propagating waves is minimal.

#### 3.3.2. Length of absorbing film

Once the thickness of the absorbing film is optimised, treating the area where the loss factors of the compound beam and beam alone coincide is not necessary. For example, at optimal thickness of  $40 \mu\text{m}$  the loss factor of the composite beam does not differ much from that of the beam alone in the area between  $x = -0.03$  and  $-0.08 \text{ m}$ , see Fig. 6. In this case the absorbing film can cover only the area of the extremum up to  $x = -0.03 \text{ m}$ . The reflection coefficient for both cases

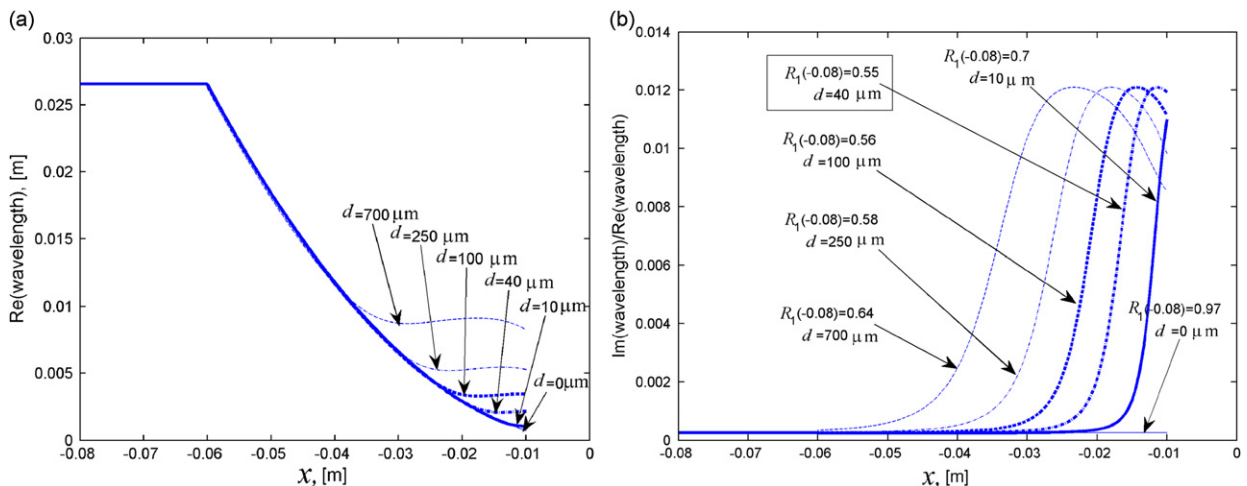
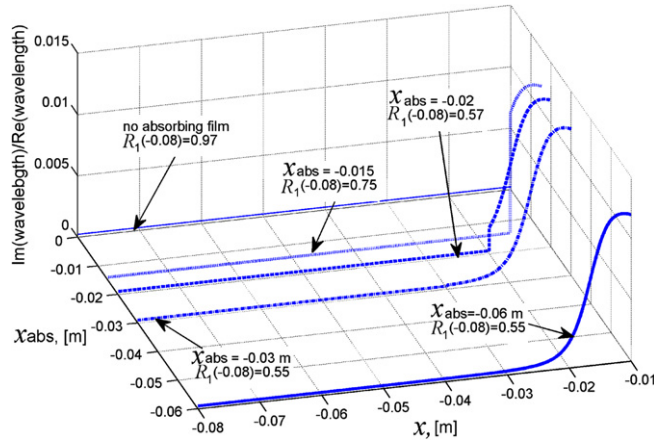
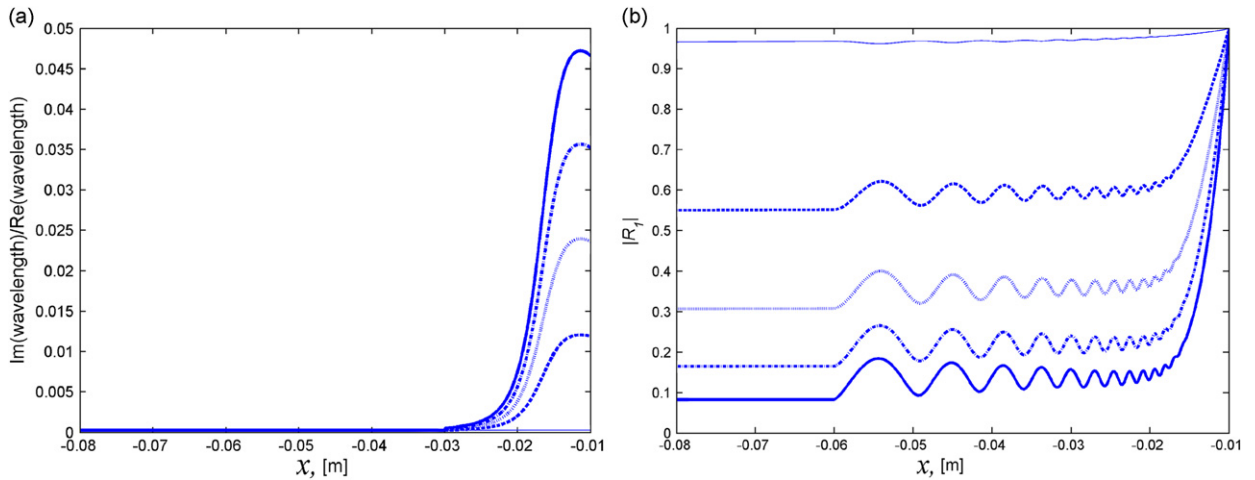


Fig. 5. (a) Real part of the wavelength and (b) ratio  $\text{Im}(\lambda(x))/\text{Re}(\lambda(x))$  of the compound beam for different thicknesses  $d$  of the absorbing film.



**Fig. 6.** Ratio  $\text{Im}(\lambda(x))/\text{Re}(\lambda(x))$  of the composite beam for different lengths of the absorbing film  $x_{\text{abs}}$ :  $x_{\text{abs}}=0$ —thin solid curve;  $x_{\text{abs}}=-0.06$  m—thick solid curve;  $x_{\text{abs}}=-0.02$  m—dashed curve;  $x_{\text{abs}}=-0.03$  m—thin dotted curve; and  $x_{\text{abs}}=-0.015$  m—thick dotted curve.



**Fig. 7.** Ratio  $\text{Im}(\lambda(x))/\text{Re}(\lambda(x))$  of the compound beam (a) and reflection coefficient  $R_1$  (b) for different values of  $\eta_2$ :  $\eta_2=0$ —thin solid curve;  $\eta_2=0.05$ —dashed curve;  $\eta_2=0.1$ —dotted curve;  $\eta_2=0.15$ —dash-dotted curve; and  $\eta_2=0.2$ —thick solid curve.

when the absorbing film covers the whole profile and when it covers only the area of the extremum do not differ significantly. However, if the treated area covers partially the extremum (e.g. from  $-0.01$  to  $-0.015$  m), the reflection coefficient increases, see Fig. 6.

### 3.3.3. Loss factor of absorbing film

Besides the thickness and length of the absorbing film, its loss factor  $\eta_2$  is another parameter that could improve the efficiency of ABH effect. Fig. 7 shows that increasing the loss factor of the absorbing film leads to direct decrease of the reflection coefficient. For example, increasing the loss factor  $\eta_2$  from 5% to 20% (Fig. 7(a)) leads to reduction of the reflection coefficient from 55% to less than 10% (Fig. 7(b)). Therefore, using highly absorbing material as a damping layer a passive absorber without added mass that is able to dissipate more than 99% of vibration energy of propagating waves could be designed.

### 3.3.4. Young's modulus of absorbing film

Young's modulus of absorbing film  $E_2$  is used in Eq. (B.1) for specifying the loss factor of compound beam. Thus, the change of  $E_2$  could be used for increasing the loss factor and its optimal localisation. Fig. 8 shows the effect of using absorbing films with different stiffness properties. The increase of Young's modulus leads to decrease of the loss factor and shift of the extremum towards the thicker part of the beam and vice versa.

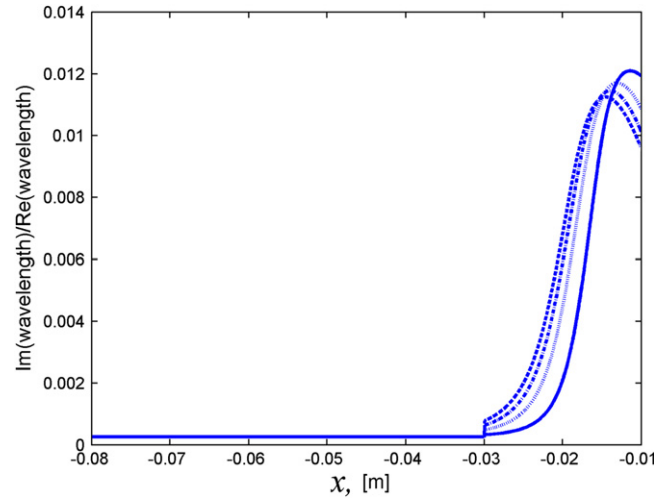


**Fig. 8.** Ratio  $\text{Im}(\lambda(x))/\text{Re}(\lambda(x))$  of the compound beam for different values of Young's modulus of absorbing film  $E_2$  in GPa:  $E_2=0.5$ —solid curve;  $E_2=1.5$ —dotted curve;  $E_2=2.5$ —dash-dotted curve;  $E_2=3.5$ —dashed curve.

## 4. Experimental investigation

### 4.1. Design and manufacture of the elliptical plate

As mentioned above, an elliptical plate has been designed and manufactured to validate the numerical method. This is possible due to the focalisation effect that allows comparing the numerical results for a beam with the experimental ones obtained by testing the elliptical plate (see Fig. 2). The parameters of the materials used can be seen in Table 1, whereas its geometrical parameters are listed in Table 2.

The manufacturing process of the elliptical plate included four stages. The first one consists of cutting and preparing the elliptical shape of the plate. In the next step, the power-law profile of ABH is created using an electro-erosion process. In the third stage, the absorbing film is placed in the area of ABH. In the last phase, the final thickness of the complete plate is achieved as in the centre of ABH a small hole is formed whose diameter defines the truncation distance.

### 4.2. Experimental results

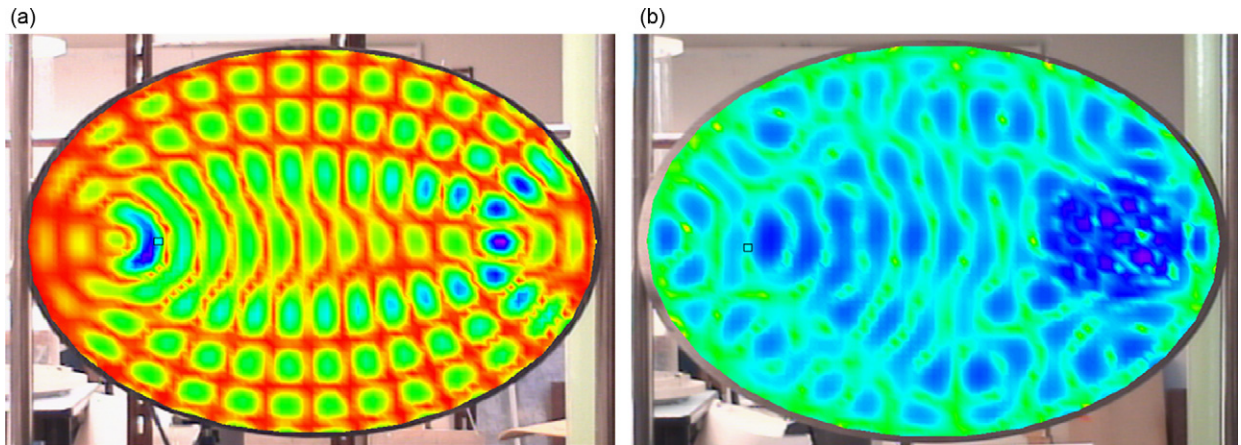
Measurements have been carried out for different replicas of the steel elliptical plate in order to demonstrate the capabilities of the proposed passive absorbing damper. The models that were tested are as follows: elliptical plate with ABH and without ABH, elliptical plate with disk of resin placed at the location of the ABH and elliptical plate completely covered by resin. The thickness of the resin is about 500  $\mu\text{m}$ . The equipment used was a Polytech Vibrometer Scanning Head—OFV 056, an impedance head Bruel&Kjaer type 8001, a Bruel&Kjaer Conditioning Amplifier, an Amplifier LM 3886, and a Shaker LDS V201. The plates were hanged vertically ('free-free' boundary conditions) and excited by the shaker using a periodic chirp signal. A number of driving-point mobilities and velocity fields were measured.

Fig. 9 shows examples of velocity fields of plates with ABH (b) and without ABH (a) at high frequencies. The excitation force was applied to the left focus, whereas the ABH is in the right one. It can be seen that the spatial patterns of the plate without ABH are rather symmetric and equally distributed with some small increases in the area of the right focus, whereas those of the plate with ABH exhibit a concentration of the velocity field in the area of ABH. This concentration is similar to the accumulation effect shown in Fig. 3. In fact, due to the focalisation, the vibration energy is guided and focused in the ABH. Thus, the rest of the plate is quite silent compared to the plate without ABH. Note that due to the focalisation effect, treating the right focus of the plate with absorbing film reduces plate vibrations as well. However, this decrease is smaller compared to the reduction of the plate with ABH and this can be seen in the measured point mobility functions.

The graphs in Fig. 10 represent driving-point mobilities at the focus of the plate where the excitation is applied. Fig. 10(a) displays the driving-point mobility of the plate with ABH and without ABH. The driving-point mobility is defined as ratio between velocity measured by the laser vibrometer and force generated by the attached shaker at the point of attachment. In the range above 5 kHz the mobility of the plate with ABH exhibits a reduction between 5 and 10 dB compared to that of the plate without ABH. This decrease is due to the focalisation and ABH effects. In Fig. 10(b) the same mobility of the plate with ABH is compared to the driving-point mobilities of plates treated with disk of resin and completely covered with resin. It is clear that in the same range above 5 kHz the driving-point mobility of the plate with ABH has the largest decrease compared to the other two. The mobility of the plate covered partially with disk of resin at the place of ABH has the least reduction. Moreover, the mobility of the absorber consisting of ABH and resin is even lower

**Table 2**  
Geometrical parameters of the elliptical plate.

Geometrical parameters of the elliptical plate, m	
$a=0.3$	$b=0.39$
$c=0.1246$	$d=0.0704$
$e=0.12$	$h_f=0.0015$



**Fig. 9.** Velocity fields of an elliptical plate: (a) without ABH at 8671 Hz and (b) with ABH at 8117 Hz.

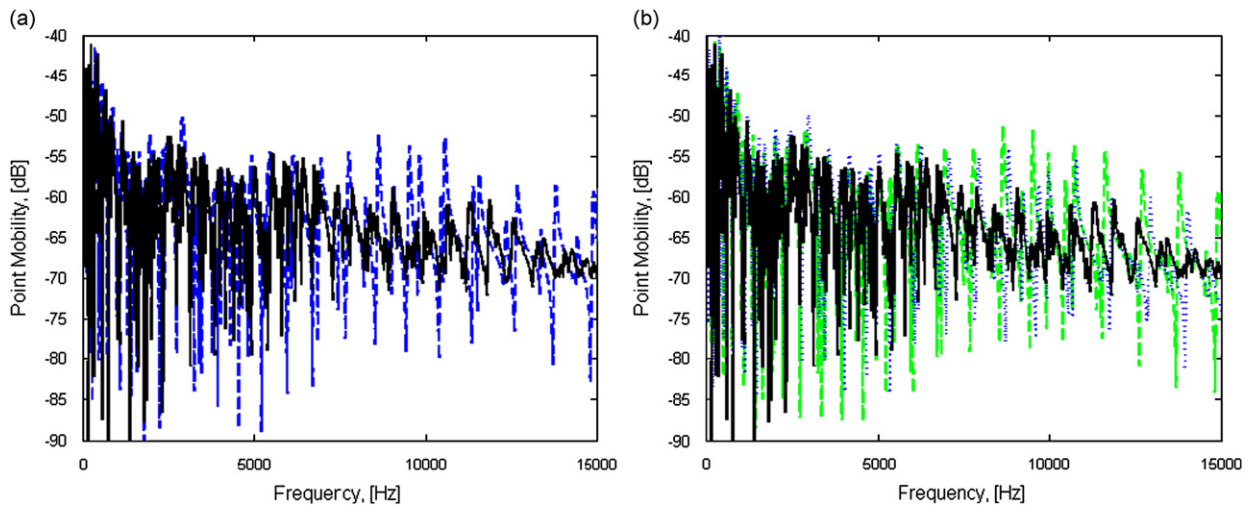


**Fig. 10.** Point mobility of an elliptical plate: (a) with ABH (solid curve) and without ABH (dashed curved) and (b) with ABH (solid curve), without ABH but with disk of resin (dashed curve) and without ABH but covered with resin (dotted curve).

compared to the one of the plate entirely covered by resin. These results can be directly related to Fig. 4, where the reflection coefficient  $R_1$  of a beam utilising ABH effect exhibits the largest reduction compared to the other beam configurations. Therefore, the proposed passive vibration damper using the ABH effect suppresses structural vibrations in high frequency range more efficiently than the traditional use of damping layers.

#### 4.3. Comparison with numerical results

The flexural waves in the 1-D ABH model shown in Fig. 1 can be generated by a single force  $F$  applied at the thicker end. The position of the force is at  $x_F = -0.25$  m, which is about the distance between two foci of the elliptical plate, see Fig. 2. The velocity of the driving point  $x_F$  can be expressed directly from Eq. (3) after that the driving-point mobility is calculated easily assuming a unit force and zero moment at the driving point. Therefore, measured driving-point mobilities of the 2-D elliptical model are compared to their corresponding mobilities of the 1-D phenomenological beam model.

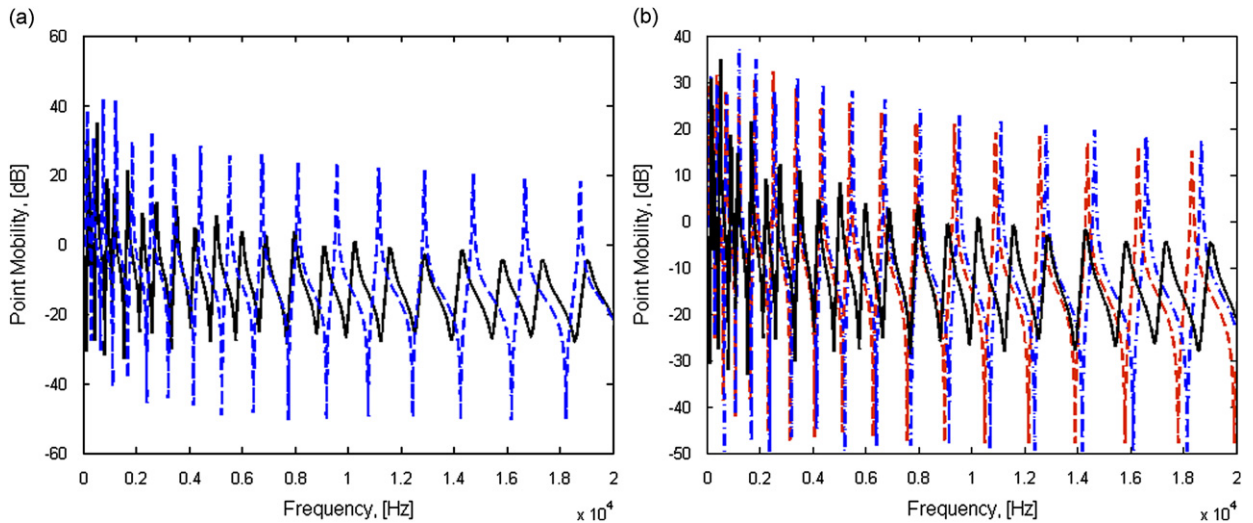


**Fig. 11.** Point mobility of a beam: (a) with ABH (solid curve) and without ABH (dashed curve) and (b) with ABH (solid curve), without ABH but with disk of resin (dash-dotted curve) and without ABH but covered entirely with resin (dashed curve).

Fig. 11(a) shows the calculated driving-point mobilities of a beam with ABH covered by an absorbing film of  $700\ \mu\text{m}$  thickness and of the same beam without ABH and without any absorbing film. It is clearly seen that there is a significant reduction of mobility function, more than 20 dB above 2 kHz due to ABH. Moreover, the introduced damping layer on the beam without ABH does not improve much its point mobility functions (see Fig. 11(b)), similarly to Fig. 10(b). For example, if the beam is partially or fully covered by an absorbing film, it does not reduce the driving-point mobility considerably. Again, this result could be linked to Fig. 4 and to the calculation of the reflection coefficient  $R_1$ . However, for the case with ABH the reduction of point mobility is unquestionable. The good overall agreement between Figs. 10 and 11 shows that approximating the dynamic behaviour of an elliptical plate by a beam does not introduce significant errors and allows for a more insight into the theory of ABH to be made.

## 5. Conclusions

In the present paper, a new alternative approach to the description of damping structural vibrations in beams and elliptical plates with acoustic black holes (ABH) has been developed and reported. The proposed methodology is based on the ABH effect for a beam with a power-law profile covered by a thin absorbing layer.

Studying a beam utilising the ABH effect, it was numerically and experimentally confirmed that an absorbing layer played a very important part in the overall design of this new type of vibration damper. On the one hand, the absorbing layer reduces the effect of decreasing the length of power-law profile, and on the other hand, it reduces the reflection of waves due to the end truncation. When applied individually, the power-law profile and the absorbing film did not reduce the reflection coefficient  $R_1$  by more than 3%, whereas when applied together this reduction was about 35%.

A parametric study was conducted in order to specify some rules for determining the optimal geometrical and material properties of the absorbing film. The main criterion for optimising the absorbing film is the loss factor of the compound beam. The extremum of the loss factor has to be positioned at the end of the beam, which specifies the thickness of the absorbing film. Covering only the area of extremum of the loss factor specifies the length of the absorbing film. Finally, the larger the loss factor of the absorbing film the smaller the reflection coefficient  $R_1$  without changing any other parameters.

The vibration velocity fields measured on elliptical plates demonstrated clearly the role of the ABH effect at one of the foci and its similarity to the ABH effect for a 1-D structure. The tests of elliptical plates utilising ABH effect show significant reduction of driving-point mobility compared to the other configurations. In the frequency range above 5 kHz, this reduction can reach about 10 dB. These results are in good agreement with the numerical calculations of reflection coefficient  $R_1$  and driving-point mobilities for beam configurations. Thus, the physics of ABH effect in elliptical plates can be successfully explained by numerical results obtained for a 1-D structure.

The above-mentioned new approach to reduction of structural vibrations in beams and elliptical plates using the acoustic black hole effect could find useful applications in aerospace and automotive industries.

## Acknowledgement

The authors wish to thank the “Région Pays de la Loire” for the financial support of the post-doctoral position of V.B. Georgiev.

**Appendix A. State vector formalism for a non-uniform beam**

*A.1. State equation and Riccati equation for the impedance of the beam*

In the framework of Euler–Bernoulli model in harmonic regime, the relationships between displacement  $w$ , slope  $\theta$ , shear force  $F$ , and bending moment  $M$  can be written in a compact form, called a state equation

$$\frac{\partial \mathbf{X}}{\partial x} = \mathbf{H}\mathbf{X}, \tag{A.1}$$

where

$$\mathbf{X} = \begin{Bmatrix} w \\ \theta \\ F \\ M \end{Bmatrix} = \begin{Bmatrix} \mathbf{x}_C \\ \mathbf{x}_F \end{Bmatrix}, \text{ and } \mathbf{H} = \left[ \begin{array}{cc|cc} 0 & 1 & 0 & 0 \\ 0 & 0 & 0 & 1/E_1 I_1 \\ -\rho_1 A_1 \omega^2 & 0 & 0 & 0 \\ 0 & 0 & -1 & 0 \end{array} \right] = \begin{bmatrix} \mathbf{H}_1 & \mathbf{H}_2 \\ \mathbf{H}_3 & \mathbf{H}_4 \end{bmatrix}, \tag{A.2}$$

$\rho_1$  is the material density of the beam,  $A_1 = bh$  is the area of the beam’s cross-section,  $E_1$  is Young’s modulus of the beam, and  $I_1 = bh^3/12$  is the moment of inertia of the beam’s cross-section.

The impedance  $\mathbf{Z}$  is defined by

$$\mathbf{x}_F = j\omega \mathbf{Z} \mathbf{x}_C, \tag{A.3}$$

where subvectors  $\mathbf{x}_C$  and  $\mathbf{x}_F$  are composed of kinematic and force components of  $\mathbf{X}$ . Replacing Eq. (A.3) into Eq. (A.1) leads to the Riccati equation

$$\frac{\partial \mathbf{Z}}{\partial x} = -\mathbf{Z}\mathbf{H}_1 - j\omega \mathbf{Z}\mathbf{H}_2 \mathbf{Z} + \frac{\mathbf{H}_3}{j\omega} + \mathbf{H}_4 \mathbf{Z}. \tag{A.4}$$

*A.2. Wave expansion of the state vector*

By stating  $\mathbf{H} = j\mathbf{N}$  it can be shown that the eigenspace of  $\mathbf{N}$  plays an important role. Considering the matrix  $\mathbf{E}$  whose columns are the eigenvectors of  $\mathbf{N}$ , and the diagonal matrix  $\mathbf{\Lambda}$  whose diagonal elements are the corresponding eigenvalues, the following equation can be written:

$$\mathbf{N}\mathbf{E} = \mathbf{E}\mathbf{\Lambda}.$$

In the case of an Euler–Bernoulli beam, the eigenvectors can be specified as follows:

$$\mathbf{E} = \left[ \begin{array}{cc|cc} j\alpha & \alpha & -j\alpha & -\alpha \\ \beta & -\beta & \beta & -\beta \\ \gamma & \gamma & \gamma & \gamma \\ -j\delta & \delta & j\delta & -\delta \end{array} \right] = \begin{bmatrix} \mathbf{E}_1 & \mathbf{E}_2 \\ \mathbf{E}_3 & \mathbf{E}_4 \end{bmatrix}, \tag{A.5}$$

where

$$\alpha = \sqrt{\frac{k_f}{\rho_1 A_1 \omega^3}}, \quad \beta = \sqrt{\frac{k_f^3}{\rho_1 A_1 \omega^3}}, \quad \gamma = \sqrt{\frac{\rho_1 A_1 \omega}{k_f}}, \quad \delta = \sqrt{\frac{\rho_1 A_1 \omega}{k_f^3}},$$

and where

$$k_f = \frac{\omega}{c_f}, \quad c_f = \sqrt[4]{\frac{E_1 I_1 \omega^2}{\rho_1 A_1}} \tag{A.6}$$

being the phase velocity.

The eigenvalues of  $\mathbf{N}$  are the wavenumbers of the beam, and  $\mathbf{\Lambda}$  is given by

$$\mathbf{\Lambda} = \text{diag}(-k_f, jk_f, k_f, -jk_f) \tag{A.7}$$

The state vector  $\mathbf{X}$  can be expressed by the matrix of eigenvectors  $\mathbf{E}$  and a wave vector  $\mathbf{V}$ , composed by forward and backward propagating structural waves,  $\mathbf{X} = \mathbf{E}\mathbf{V}$ .

*A.3. Specifying the reflection matrix  $\mathbf{R}$*

As was mentioned above, the state vector can be expressed by eigenvectors and wave vector

$$\mathbf{X} = \begin{Bmatrix} \mathbf{x}_C \\ \mathbf{x}_F \end{Bmatrix} = \mathbf{E}\mathbf{V} = \begin{bmatrix} \mathbf{E}_1 & \mathbf{E}_2 \\ \mathbf{E}_3 & \mathbf{E}_4 \end{bmatrix} \begin{Bmatrix} \mathbf{V}_f \\ \mathbf{V}_b \end{Bmatrix}. \tag{A.8}$$

To determine the reflection matrix  $\mathbf{R}$  one can use the fact that the backward propagating wave is a product of the reflection coefficient and the forward propagating wave, therefore

$$\mathbf{V} = \begin{Bmatrix} \mathbf{V}_f \\ \mathbf{V}_b \end{Bmatrix} = \begin{Bmatrix} \mathbf{V}_f \\ \mathbf{R}\mathbf{V}_f \end{Bmatrix}. \quad (\text{A.9})$$

From Eqs. (A.3), (A.8) and (A.9) the following equation can be derived:

$$\mathbf{R} = [\mathbf{j}\omega\mathbf{Z}\mathbf{E}_2 - \mathbf{E}_4]^{-1} [\mathbf{E}_3 - \mathbf{j}\omega\mathbf{Z}\mathbf{E}_1]. \quad (\text{A.10})$$

Similarly, the impedance  $\mathbf{Z}$  can be specified in the form

$$\mathbf{Z} = \frac{1}{\mathbf{j}\omega} [\mathbf{E}_3 + \mathbf{E}_4\mathbf{R}][\mathbf{E}_1 + \mathbf{E}_2\mathbf{R}]^{-1}. \quad (\text{A.11})$$

## Appendix B. Specifying the effect of absorbing film.

In the case of extensional damping (no constraining layer), the complex bending stiffness of the composite two-layered structure (beam+absorbing film) can be expressed as a function of the bending stiffness of the beam [5]

$$EI(1 + \mathbf{j}\eta) = E_1 I_1 \left[ (1 + \mathbf{j}\eta_1) + e_2 h_2^3 (1 + \mathbf{j}\eta_2) + \frac{3(1 + h_2)^2 e_2 h_2 [1 - \eta_1 \eta_2 + \mathbf{j}(\eta_1 + \eta_2)]}{1 + e_2 h_2 (1 + \mathbf{j}\eta_2)} \right], \quad (\text{B.1})$$

where  $EI$  is the bending stiffness of the composite beam (beam+absorbing film);  $E_1 I_1$  is the bending stiffness of the beam only;  $\eta$  is the loss factor of the composite beam;  $\eta_1$  is loss factor of the beam's material;  $\eta_2$  is the loss factor of absorbing film's material;  $E_1$  and  $E_2$  are Young's moduli of beam's and absorbing film's materials, respectively;  $e_2 = E_2/E_1$ ;  $d$  is the thickness of the absorbing film;  $h$  is the local thickness of the beam;  $h_2 = d/h$ .

In the case when the thickness of absorbing film is comparable to the local thickness of the beam the mass of the absorbing film also should be taken into account, thus, the mass per unit length should be

$$\rho A = \rho_1 A_1 + \rho_2 A_2, \quad (\text{B.2})$$

where  $\rho_1$  and  $\rho_2$  are beam's and absorbing film's material densities, respectively;  $A_1$  and  $A_2 = bd$  are beam's and absorbing film's cross-sections, respectively;  $b$  is the width of the beam.

Finally, replacing Eqs. (B.1) and (B.2) into the expression for phase velocity given in Eq. (A.6), one can obtain the phase velocity and wavenumber when the effect of absorbing film is introduced

$$c_f = \sqrt[4]{\frac{EI(1 + \mathbf{j}\eta)\omega^2}{\rho A}}, \quad k_f = \frac{\omega}{c_f} = \sqrt[4]{\frac{\rho A \omega^2}{EI(1 + \mathbf{j}\eta)}}. \quad (\text{B.3})$$

## References

- [1] M.A. Mironov, Propagation of a flexural wave in a plate whose thickness decreases smoothly to zero in a finite interval, *Soviet Physics—Acoustics* 34 (1988) 318–319.
- [2] V.V. Krylov, F.J.B.S. Tilman, Acoustic 'black holes' for flexural waves as effective vibration dampers, *Journal of Sound and Vibration* 274 (2004) 605–619.
- [3] V.V. Krylov, New type of vibration dampers utilising the effect of acoustic 'black holes', *Acta Acustica United with Acustica* 90 (5) (2004) 830–837.
- [4] V.V. Krylov, R.E.T.B. Winward, Experimental investigation of the acoustic black hole effect for flexural waves in tapered plates, *Journal of Sound and Vibration* 300 (2007) 43.
- [5] D. Ross, E.E. Ungar, E.M. Kerwin Jr., Damping of plate flexural vibrations by means of viscoelastic laminae, in: J.E. Ruzicka (Ed.), *Structural Damping*, Pergamon Press, Oxford 1960, pp. 49–87.
- [6] V. Kralovic, V.V. Krylov, Damping of flexural waves in tapered rods of power law profile: experimental studies, *Proceedings of the Institute of Acoustics* 29 (Part 5) (2007) 66–73.
- [7] V. Kralovic, V.V. Krylov, Some new methods of damping impact-induced vibrations in badminton racquets, *Proceedings of the Institute of Acoustics* 30 (Part 2) (2008) 66–73.
- [8] F. Gautier, J. Cuenca, V.V. Krylov, L. Simon, Experimental investigation of the acoustic black hole effect for vibration damping in elliptical plates, *Proceedings of the Acoustic'08*, Paris, June 29–July 4, 2008.
- [9] C. Vemula, A.N. Norris, G.D. Cody, Attenuation of waves in plates and bars using a graded impedance interface at edges, *Journal of Sound and Vibration* 196 (1996) 107–127.
- [10] M. Géradin, D. Rixen, *Mechanical Vibrations—Theory and Application to Structural Dynamics*, second ed., John Wiley & Sons, 1997.
- [11] Z. Wang, A.N. Norris, Waves in cylindrical shells with circumferential submembers: a matrix approach, *Journal of Sound and Vibration* 181 (3) (1995) 457–484.
- [12] F. Gautier, M.H. Moutlet, J.C. Pascal, Reflection, transmission and coupling coefficients of longitudinal and flexural wave at beams junctions—part I: measurement methods, *Acta Acustica United with Acustica* 92 (2006) 982–997.
- [13] S. Félix, V. Pagneux, Multimodal analysis of acoustic propagation in three-dimensional bends, *Wave Motion* 36 (2002) 157–168.
- [14] D.R. Kincaid, E.W. Cheney, *Numerical Analysis—Mathematics of Scientific Computing*. Brooks Cole, 1996.
- [15] C.F. Gerald, P.O. Wheatley, *Applied Numerical Analysis*, Addison-Wesley, 1999.